Kinetics and Activation Thermodynamics of Methane Monooxygenase Compound **Q** Formation and Reaction with Substrates†

Brian J. Brazeau and John D. Lipscomb*

Department of Biochemistry, Molecular Biology, and Biophysics, and the Center for Metals in Biocatalysis, University of Minnesota, Minneapolis, Minnesota 55455

Received June 27, 2000; Revised Manuscript Received August 24, 2000

ABSTRACT: The transient kinetics of formation and decay of the reaction cycle intermediates of the *Methylosinus trichosporium* OB3b methane monooxygenase (MMO) catalytic cycle are studied as a function of temperature and substrate type and deuteration. Kinetic evidence is presented for the existence of three intermediates termed compounds **O**, **P***, and **P** forming after the addition of O_2 to diferrous MMO hydroxylase (**H**^{r}) and before the formation of the reactive intermediate compound **Q**. The Arrhenius plots for these reactions are linear and independent of substrate concentration and type, showing that substrate does not participate directly in the oxygen activation phase of the catalytic cycle. Analysis of the transient kinetic data revealed only small changes relative to the weak optical spectrum of **H**^{r} for any of these intermediates. In contrast, large changes in the 430 nm spectral region are associated with the formation of **Q**. The decay reaction of **Q** exhibits an apparent first-order concentration dependence for all substrates tested, and the observed rate constant depends on the substrate type. The kinetics of the decay reaction of **Q** yield a nonlinear Arrhenius plot when methane is the substrate, and the rates in both segments of the plot increase linearly with methane concentration. Together these observations suggest that at least two reactions with a methane concentration dependence, and perhaps two methane molecules, are involved in the decay process. When CD_4 is used as the substrate, a large isotope effect and a linear Arrhenius plot are observed. Analogous plots for all other MMO substrates tested (e.g., ethane) are linear, and no isotope effect for deuterated analogues is observed. This demonstrates that a step other than C−H bond breaking is rate limiting for alternative MMO substrates. A two step **Q** decay mechanism is proposed that provides an explanation for the lack of an isotope effect for alternative MMO substrates and the fact that rate of oxidation of methane by **Q** exceeds that of many other hydrocarbons with weaker C−H bonds.

Methanotrophic bacteria utilize methane as the sole source of carbon and energy (*1*, *2*). The type II methanotroph *Methylosinus trichosporium* OB3b expresses a soluble methane monooxygenase (MMO OB3b)[1] which catalyzes the first step of the oxidative degradation of methane, the conversion of methane to methanol (*3*, *4*). Soluble methane monooxygenases have also been purified from other sources (*1*, *4*−*6*), including the type X methanotroph *Methylococcus capsulatus* Bath which expresses an enzyme (MMO Bath) very similar to MMO OB3b despite substantial differences in cellular morphology of the bacteria and the optimal growth temperature for each strain (*7*−*9*). Several other oxygen activating enzymes are now known to possess structural and mechanistic similarities to MMO (*10*−*14*).

The MMO system consists of three component proteins, a hydroxylase (MMOH), a reductase, and a regulatory protein termed component B (MMOB) (*3*, *15*). The hydroxylase is a dimer in which each protomer has an ($\alpha\beta\gamma$) subunit structure (*16*, *17*). An oxygen bridged binuclear iron site that is required for oxygen activation and substrate oxidation is sequestered in each α subunit (*18*). Both iron atoms in MMOH as isolated are in the Fe(III) state and must be reduced to Fe(II) to react with oxygen (*3*, *18*). The NADH-coupled reduction is catalyzed by MMO reductase, which contains FAD and a [2Fe-2S] cluster (*3*, *19*). MMOB affects the kinetics, regiospecificity, and spectral properties of MMOH when it forms a specific complex with the α-subunit of this component (*20*−*24*). To date, the most important effect of MMOB is a 1000-fold increase in the rate of the reaction between oxygen and MMOH to yield an oxygen complex of the binuclear iron site (*23*).

Single turnover studies in which the chemically reduced MMOH in the presence of MMOB (1:1 with MMOH active sites) is mixed with O_2 have led to the proposed mechanism shown in Scheme 1 (*3*, *4*, *25*−*27*). The diferrous [Fe(II)Fe(II)] form of MMOH (**H**^{r}) reacts with O_2 to form compound **O** (**O**) in which the oxygen is proposed to bind to the enzyme but not to the dinuclear iron center. **O** decays to compound **P*** (**P***) with the loss of an EPR signal at $g = 16$ that is characteristic of the diferrous cluster (*18*, *26*). Consequently, **P*** is likely to be an oxygen complex of the cluster in which electron density moves from the irons to the oxygen to yield

† This work was supported by NIH Grant GM40466. B.J.B. was supported in part by NIH Training Grant GM08700.

* To whom correspondence should be addressed. Phone: (612) 625-6454. Fax: (612) 625-2163. E-mail: lipsc001@tc.umn.edu.

[1] Abbreviations: D, ^{2}H; KIE, kinetic isotope effect; MMO, methane monooxygenase; MMOH, MMO hydroxylase component; MMOB, MMO component B; MOPS, 3-[*N*-morpholino]propane-sulfonic acid; P450, cytochrome P450 monooxygenase; **H**^{r}, reduced MMOH; **O**, **P***, **P**, **Q**, **T**, compounds **O**, **P***, **P**, **Q**, **T** of the MMOH catalytic cycle.

10.1021/bi001473l CCC: $19.00
Published on Web 10/13/2000

Scheme 1: Proposed Reaction Cycle for MMOH[a]

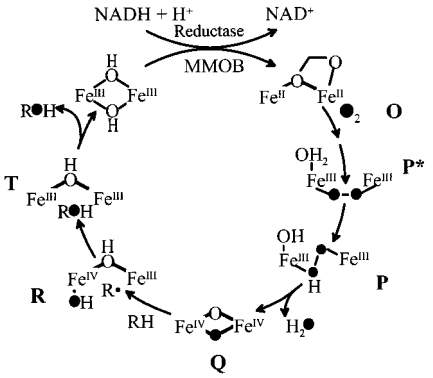

[a] The filled oxygen atoms represent our current understanding of the fate of the atoms derived from O_2. The structures of the intermediates **O** through **T** are based on spectroscopic and model studies.

a diferric [Fe(III)Fe(III)] or mixed valence [Fe(II)Fe(III)] cluster. **P*** decays to compound **P** (**P**) which has been shown to have a diferric cluster by Mössbauer spectroscopy (*22*, *28*). Both the Mössbauer parameters and the chromophoric properties of **P** suggest that it is a diferric peroxy species. Because a proton appears to be required for formation of **P** (*26*), it is possible that both **P*** and **P** are peroxy species, but the oxygen in **P** is protonated in preparation for cleavage of the O−O bond. **P** spontaneously converts to the bright yellow intermediate compound **Q** (**Q**) in a reaction that also requires a proton (*26*, *27*). **Q** has been shown to react with methane to yield methanol (*27*). Mössbauer spectra of **Q** show that each iron of the diiron cluster is in the Fe(IV) state (*28*, *29*). Moreover, EXAFS experiments suggest that the O−O bond is broken in **Q** and at least two single atom oxygen bridges link the irons of the cluster, forming a "diamond core" structure (*28*). Electronically equivalent, but structurally distinct, ferryl-oxo species have been proposed as reactive intermediates in the reactions of the heme containing oxygenases cytochrome P-450 (P450) and nitric oxide synthase (*30*−*33*). This type of intermediate has also been trapped and characterized as compound I of heme containing peroxidases (*31*). However, **Q** is the first non-heme ferryl-oxo species to have been identified in biological systems and the only binuclear Fe(IV) species known. Of the intermediates proposed in the oxygen activation sequence of MMO, only **P** and **Q** have distinct visible chromophores that allow them to be directly detected. Intermediates **O** and **P*** have been proposed based on indirect kinetic evidence. In the current study, the first direct evidence for these species is presented.

The reaction of **Q** with unactivated hydrocarbon substrates, and the ability to observe this reaction due to the favorable kinetics and intense chromophore of the intermediate, provides a unique opportunity to investigate this important chemistry. The reaction of **Q** with substrates is unusual in several respects. First, our initial studies of the MMO reaction cycle kinetics showed that only the decay of compound **Q** is substrate concentration dependent (*27*). The **Q** formation reaction, like all of the preceding reactions in the single turnover cycle, was found to be insensitive to substrate, suggesting that substrate first enters the reaction cycle after the formation of **Q**. This differs from the reactions of enzymes such as P450 in which substrate binding plays an important role in initiation of the catalytic cycle (*34*). Second, the reaction of **Q** with substrates was found not to saturate in contrast to the usual enzyme−substrate reaction (*27*). Finally, the reaction with methane was shown to exhibit a primary deuterium isotope effect in the range of 50−100 (*35*). This is among the largest values observed for a biological system and is much larger than the isotope effects determined for steady-state reactions of similar MMO substrates such as ethane (KIE ≈ 4) (*36*). This suggests that methane reacts by a mechanism that differs somewhat from that of other hydrocarbons, perhaps one involving quantum mechanical hydrogen tunneling.

One approach to the investigation of the reactions of **Q** has been to determine the activation thermodynamic parameters for its formation and decay reactions. Our previous determination of the temperature dependence of the formation (**k_{QF}**) and decay (**k_{QD}**) rate constants using MMOH isolated from MMO OB3b in the presence of methane in the range of 4−17 °C showed linear Arrhenius plots that revealed a higher activation energy for **P** decay (**Q** formation) than **Q** decay (*35*). In a recent study of MMOH isolated from MMO Bath, Valentine et al. (*37*) studied the reaction at temperatures up to 39 °C and reported that this enzyme exhibits the same relationship for the relative magnitudes of the activation energies for **P** and **Q** decay reactions, suggesting that the underlying chemistry of the oxygen activation reactions of the MMO enzymes from these quite divergent organisms are similar.

In the current study, the rates of the reactions leading from $\mathbf{H^r}$ to the formation and subsequent decay of **Q** have been determined for MMOH OB3b as a function of temperature and the concentration, type, and deuteration of the substrate. Data were obtained for a variety of substrates over a much wider temperature range than in our preliminary study and the activation thermodynamic parameters were determined for each reaction. For the reactions of most substrates with **Q**, linear Arrhenius plots were obtained. However, uniquely in the case of methane, nonlinear Arrhenius plots were observed, suggesting for the first time that the **Q** reaction with substrate involves more than one step. The new complexity in the reaction of **Q** with methane revealed by this study may help to account for many long-standing anomalies in MMO catalysis including the lack of saturation behavior in the reaction of substrates with **Q** and the remarkable observation that the stable C−H bond of methane appears to be cleaved faster than most weaker C−H bonds in adventitious substrates.

EXPERIMENTAL PROCEDURES

Enzyme Purification. MMOH was purified as previously described from *Methylosinus trichosporium* OB3b (*3*, *38*) with the following modification. As a result of scaling-up the purification, the fractions of the eluant from the first DEAE column which contained MMOH activity were found to have a significant increase in pH. Neutralization was achieved by the addition of one-fifth of the fraction volume of 500 mM MOPS, pH 7. Recombinant MMOB was purified as previously described (*39*).

Chemicals. All chemicals were purchased from Sigma, Aldrich, or ICON and used without purification. Water was deionized and then purified using a Millipore reverse osmosis system. Substrate solutions were prepared by bubbling gas

for 1 h into 2 mL of 50 mM MOPS, pH 7. The solutions were determined to be saturated by GC analysis. The concentrations of the saturated methane, ethane, and propane solutions were 1.5, 2.1, and 2.9 mM, respectively, at 25 °C (Merck Index).

Stopped-Flow Experiments. Single-turnover reactions of MMOH were monitored using a stopped-flow apparatus from Applied Photophysics (model SX.18MV). The sample preparation has been reported previously (*26*, *27*). In brief, MMOH was made anaerobic and subsequently reduced with methyl viologen and stoichiometric dithionite to yield the 2 electron reduced state. It was then transferred to the stopped-flow using a Hamilton gastight syringe. The other stopped flow syringe was loaded with MMOB, oxygen saturated (∼1.4 mM) buffer, and the appropriate substrate. The samples were then rapidly mixed (1:1) and the absorbance changes were followed at a fixed wavelength. The mixed concentration of MMOH was 25 μM active sites and MMOB was 27 μM except in Figure 1 where half these values were used.

The buffer for all experiments was 50 mM MOPS, pH 7. In temperature dependent experiments, the temperature was adjusted by a circulating water bath. Before rapidly mixing at a new temperature, the samples were allowed to equilibrate for 15 min.

In the sequential-mix stopped-flow experiments, intermediate **Q** was formed by mixing $\mathbf{H^r}$ with a saturated O_2 and MMOB solution as described above and then allowed to accumulate in a mixing chamber prior to being rapidly mixed with methane solution. The time when the second mixing operation was initiated at each temperature was that at which **Q** was maximally formed in single-turnover reactions in the absence of substrate at the same temperature.

Data Analysis. Pseudo-first-order kinetics were generally observed because O_2 adds in an effectively irreversible step in the dead time of the stopped flow instrument for all experiments and the substrate concentrations are in large excess over that of MMOH for most experiments. The reactions followed usually consisted of at least two steps, resulting in at least two kinetic phases in the time course. The phases sum together to produce the overall time course. The number of relaxations observed defines the minimum number of steps in the reaction, but it does not define a specific mechanism or order for the steps. In the current case, rapid scan optical and time-resolved Mössbauer spectroscopies (*27*−*29*) have shown that **P** forms prior to **Q**. If it is assumed that the steps are irreversible, then the relaxation times are equal to the reciprocal rate constants for the steps. Finally, amplitude analysis has been used to identify which relaxation time is associated with the formation of **Q** (*27*). The reciprocal relaxation times and the amplitudes of each phase were determined using the nonlinear regression fitting program KFIT developed by Neil. C. Millar (King's College London, U.K.).

The assignment of the reciprocal relaxation times determined using a summed three exponential fit at 430 nm for the reaction sequence leading to **Q** formation and decay was based on the fact that only the rate of **Q** decay has been shown to be accelerated by the presence of substrates (*27*, *35*). Thus, as the concentration of substrate was varied, the rate constant of **Q** decay was identified as the reciprocal relaxation time that changed while the other two rate constants were assigned to **Q** and **P*** formation.

Fitting transient kinetic data to three or more exponential phases is prone to error because false minima are easily found by nonlinear regression programs. We found it necessary to use a fitting program that allowed the entry of a series of different initial estimates for the kinetic parameters so that many fits could be compared. For example, fits of the data such as that shown in Figure 2 required the initial input of a negative amplitude for the first phase because this solution was never selected when the same data were analyzed using fitting programs that automatically generate parameter estimates. The improvement in the residual error of the fit using systematic variation of starting parameters was dramatic, and the fact that a nearly error-free fit could be obtained over three kinetic phases with rate constants encompassing a 4 order of magnitude range enhanced our confidence in the values of the parameters determined. The use of other information such as analysis of the kinetic time course at several different wavelengths and differences in concentration dependence of the various kinetic phases was also found to be essential in the determination of accurate kinetic parameters.

Singular value decomposition (SVD) analysis of diode array detected stopped-flow experiments was performed using the software package ProK supplied by Applied Photophysics.

Temperature-Dependent Analysis. The natural log of the reciprocal relaxation time was plotted against the reciprocal of the absolute temperature. The data were then fit to the Arrhenius equation (eq 1) using the linear fitting function in the plotting program Origin (Microcal):

$$\ln k = \ln A - E_a/RT \tag{1}$$

where A is the Arrhenius preexponential factor and R is the gas constant. The position of the break point in the nonlinear Arrhenius plots was found by fitting the high and low-temperature regions of the Arrhenius plot separately.

The activation enthalpy, activation entropy, and Gibbs' free energy of activation were determined using eqs 2, 3, and 4, respectively, where k_B is the Boltzmann constant and h is Planck's constant.

$$\Delta H^{\ddagger} = E_a - RT \tag{2}$$

$$\Delta S^{\ddagger} = R[\ln A - \ln(k_B T/h)] \tag{3}$$

$$\Delta G^{\ddagger} = \Delta H^{\ddagger} - T\Delta S^{\ddagger} \tag{4}$$

Simulations. Simulations of the kinetic time course for the reaction model given in the text (see Scheme 3) were performed using the numerical integration kinetic simulation program KSIM (provided by Neil. C. Millar). The Arrhenius equation was used to predict a set of rate constants for each temperature by using the activation energy and preexponential factor from each region of the experimental Arrhenius plot for the reaction in which 200 μM methane (and the standard 25 μM $\mathbf{H^r}$) was present. It was assumed that the inherent reactions in each temperature region would each give a linear Arrhenius plot. The data for other concentrations of methane were simulated using the same set of rate constants scaled linearly for the methane concentration for the constants that were assumed to be first order in methane.

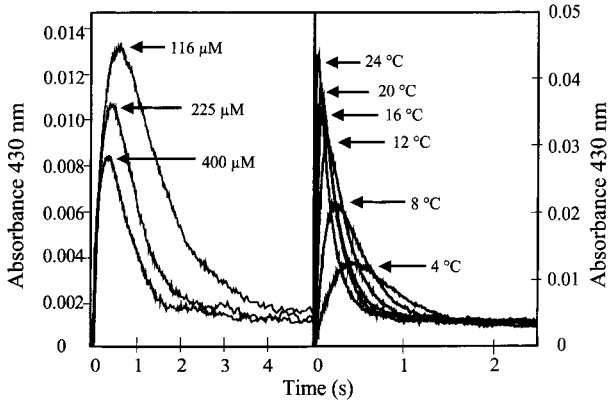

FIGURE 1: Time course of **Q** formation and decay as a function of temperature and methane concentration observed at 430 nm in a stopped-flow spectrophotometer with a single wavelength detector. The single-turnover reaction conditions are described in Experimental Procedures. (A) The effects of methane concentration on the **Q** time course were observed at pH 7, 4 °C. Similar plots are obtained at higher temperatures. (B) The effects of temperature. The concentration of methane was 200 μM at pH 7.

The simulated time course was then fit using KFIT as if the **Q** decay reaction occurred in a single step, i.e., in the same way as the experimental data were analyzed.

RESULTS

Overall Reaction Time Course. The overall changes in the time course of the formation and decay of the chromophoric intermediate **Q** in response to changes in temperature and substrate concentration are shown in Figure 1. Changes in both the maximum concentration of **Q** ($\boldsymbol{Q}_{max}$) and the time at which the maximum is reached (t_{max}) are apparent. These trends are readily understood if the simplest case, a two irreversible step reaction (**P** → **Q** → **T** where k_{QF} and k_{QD} are the first and second rate constants, respectively), is considered (eq 5). In this case, t_{max} and $\boldsymbol{Q}_{max}$ are given by eqs 6 and 7, respectively:

$$\boldsymbol{Q}_t = A_0\{[k_{QF}/(k_{QD} - k_{QF})]e^{-t/\tau_1} + [k_{QF}/(k_{QF} - k_{QD})]e^{-t/\tau_2}\} \quad (5)$$

$$t_{max} = [1/(k_{QD} - k_{QF})]\ln(k_{QD}/k_{QF}) \quad (6)$$

$$\boldsymbol{Q}_{max} = A_0(k_{QF}/k_{QD})^{[k_{QD}/(k_{QD}-k_{QF})]} \quad (7)$$

where $\boldsymbol{Q}_t$ is the concentration of **Q** at time *t*. In eq 5 and 7, A_0 is the concentration of the dinuclear iron sites in the experiment. The reciprocal of the relaxation times τ_1 and τ_2 are equal to the rate constants k_{QF} and k_{QD}, respectively, as long as the steps are effectively irreversible. The maximum absorbance observed is proportional to the $\boldsymbol{Q}_{max}$ if **Q** is assumed to be the only chromophoric species. It can be seen from Figure 1 that there is a small increase in absorption at 430 nm between the beginning and end of the reaction, thus **Q** is not the only chromophoric species, but it is by far the largest contributor to the absorbance (see below). Because the formation of **Q** appears to involve fissure of the O−O bond (*26*, *28*) and oxygen is inserted into a C−H bond during the breakdown of **Q** (*27*, *35*), the assumption of irreversibility is probably also valid.

Increase in either methane concentration or temperature causes t_{max} to decrease which indicates that k_{QF} and/or k_{QD} are increased (eq 6). The fact that $\boldsymbol{Q}_{max}$ increases with increasing temperature shows that k_{QF} increases faster than k_{QD} (eq 7). Thus, the activation energy for **Q** formation (**P** decay) is larger than that for **Q** decay. In contrast, the fact that $\boldsymbol{Q}_{max}$ decreases with increasing methane concentration shows that k_{QD} increases faster than k_{QF} (eq 6). Thus, methane concentration has a significantly larger effect on **Q** decay than **Q** formation (**P** decay). Indeed, both our previous studies (*27*) and the studies reported below show that only the **Q** decay reaction is dependent on methane concentration.

Temperature Dependence and the Effect of Substrate Type and Concentration the Rate Constants in the Q Formation Sequence. Although the simple assumption of a two step irreversible reaction allows a reasonably good fit of the reaction time course, our recent studies have shown that there are at least two intermediates (**O** and **P***) before **P** in the reaction cycle as illustrated in Scheme 2 (*26*). The advent

Scheme 2: Intermediates and Rate Constant Nomenclature

$$\mathbf{O} \xrightarrow{k_{P^*F}\,(=k_{OD})} \mathbf{P^*} \xrightarrow{k_{PF}\,(=k_{P^*D})} \mathbf{P} \xrightarrow{k_{QF}\,(=k_{PD})} \mathbf{Q} \xrightarrow{k_{QD}} \mathbf{T} \xrightarrow{k_{TD}} \mathbf{H_{ox}}$$

of stopped flow instrumentation with a very short dead time now allows the effect of these early fast reactions on the **Q** time course to be monitored. In principle, five exponential phases would be required to fit the time course for the reaction: $\mathbf{H^r} \rightarrow \mathbf{O} \rightarrow \mathbf{P^*} \rightarrow \mathbf{P} \rightarrow \mathbf{Q} \rightarrow \mathbf{T}$. However, as shown in Figure 2, excellent fits were obtained using only three exponentials for the data from the reaction monitored at 430 nm suggesting that two phases were not observed. Past studies indicate that **O** is formed in the dead time of the stopped flow and that it probably has essentially the same UV−vis spectrum as diferrous MMOH accounting for one of the missing phases (*23*). We believe that the second missing phase is that with a reciprocal relaxation time equal to the formation rate constant of **P** for reasons that will be explained below. Consequently, the data were fit with a three irreversible step model (**O** → **P*** → **Q** → **T**) so that the values of k_{P^*F} (= k_{OD}), k_{QF} (= k_{PD}), and k_{QD} are each given by one of the reciprocal relaxation times of the three summed exponentials necessary to fit the data (see Experimental Procedures). Often it is difficult to obtain reliable fits for data requiring a three exponential equation, especially if the rate constants are similar. In the current case, the amplitudes of exponentials alternate between negative and positive for each phase when measured at 430 nm, greatly facilitating the analysis and allowing excellent fits to the data as illustrated in Figure 2, panels A and B. The data indicate that the first phase has a small negative amplitude[2] that is easily observed for data from reactions run at higher

[2] Analytical amplitudes of kinetic phases in multistep reactions may have the opposite sign of the direction of absorbance change observed depending upon the relative magnitude of the rate constants and whether the species being formed has a larger extinction coefficient than the starting species. This is so because contribution of the rapidly decaying phase with a negative amplitude is summed with a more slowly decaying phase with a positive amplitude to give a net positive concentration (absorbance) of the intermediate decaying or being formed. Nevertheless, to avoid confusion, we will refer to the amplitudes by the observed direction of change.

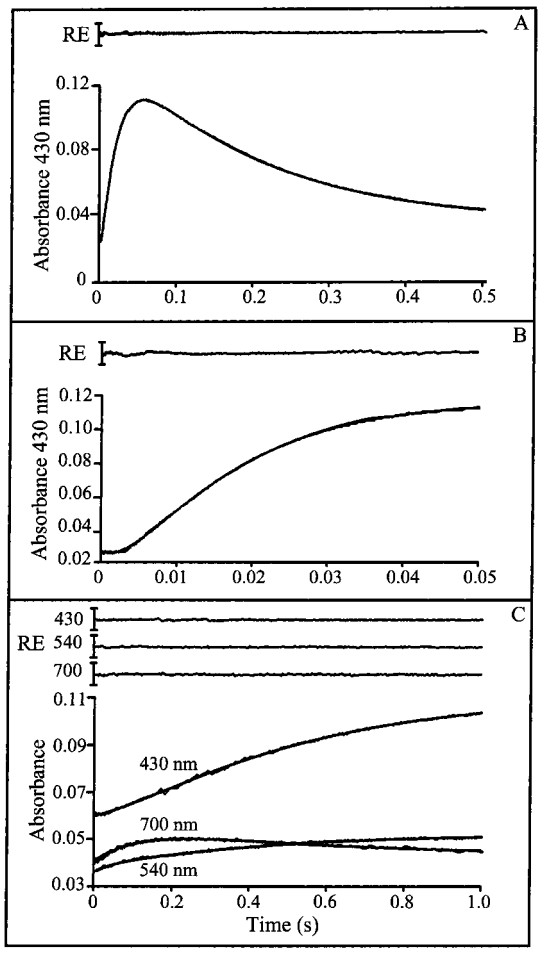

FIGURE 2: Typical fit of the time course of **Q**. Shown in panels A and B are both the data and fit (superimposed smooth solid line) of the reaction between reduced MMOH and O_2 plus MMOB in the presence of 100 μM methane at pH 7, 25.9 °C using a single wavelength detector. The experiment and the fitting procedures are described in Experimental Procedures. The entire time course was accurately fit by a summed three-exponential equation as shown by the residual above each time course. The residual error (RE) is plotted on the same scale as the data. Fit parameters: $k_1 = 270$ s^{-1}, $Amp_1 = -0.036$; $k_2 = 50$ s^{-1}, $Amp_2 = 0.16$; $k_3 = 5.2$ s^{-1}, $Amp_3 = -0.118$. (A) Entire time course monitored at 430 nm. (B) The first 50 ms of the time course shown in (A). Note the lag caused by the early kinetic phase with a negative amplitude. (C) Comparison of the first 1 s of the reaction between reduced MMOH and O_2 in the absence of a substrate at pH 7, 4 °C. Time courses are shown for the reaction monitored at 430, 540, and 700 nm, respectively. Fit parameters: (430 nm) $k_1 = 22$ s^{-1}, $Amp_1 = -0.006$; $k_2 = 1.7$ s^{-1}, $Amp_2 = 0.064$; (540 nm) $k_1 = 28$ s^{-1}, $Amp_1 = 0.003$; $k_2 = 9$ s^{-1}, $Amp_2 = -0.002$; $k_3 = 2.5$ s^{-1}, $Amp_3 = 0.014$; (700 nm) $k_1 = 29$ s^{-1}, $Amp_1 = -0.004$; $k_2 = 12$ s^{-1}, $Amp_2 = 0.017$; $k_3 = 2.5$ s^{-1}, $Amp_3 = -0.010$.

temperatures (Figure 2, panels A and B), but is required to fit the data at all temperatures (Figure 2C). At 4 °C, pH 7, this fast phase occurs with a rate of 22 ± 4 s^{-1}. This rate is in accord with our previous determination of the formation rate of **P*** (26 s^{-1}, at pH 7.0) from direct observation of the decay of the $g = 16$ EPR signal from the integer spin state of **O** (and $\mathbf{H}^r$) (*23*, *26*, *27*). Thus, it appears to be correct that **O** is nearly completely formed in the dead time of the experiment and the sequence of observed intermediates shown above is justified. This first phase has not been previously observed, and it is in a time domain where artifacts are common. However, if the same reaction is

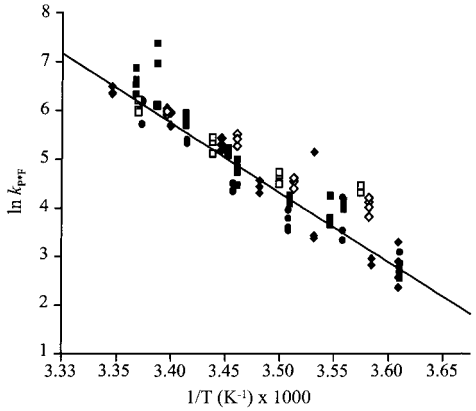

FIGURE 3: Arrhenius plot of the rate constant of **P*** formation (k_{P*F}). Diferrous, anaerobic MMOH was reacted with MMOB, O_2, and the appropriate substrate and monitored at 430 nm in a stopped-flow device. The first-order rate constant was derived at each temperature from the most rapid phase of a summed-three exponential fit as described in Experimental Procedures. The reaction was observed for the following substrates: (■) no substrate, (♦) 100 μM methane, (●) 400 μM methane, (◊) 360 μM propene, and (□) 400 μM furan. At minimum, each experiment was performed and plotted in triplicate. The slope of the linear fit to the data was used to calculate the activation energy and other activation parameters.

monitored at 540 nm (Figure 2C) the same phase is observed with a positive rather than a negative amplitude suggesting that this phase is indeed part of the time course of **Q** formation. The first phase becomes very fast as the temperature is increased (e.g., Figure 2B) and comparatively few data points could be obtained relative to the number of points for succeeding phases. Consequently, the activation parameters determined have substantial error. Nevertheless, the Arrhenius plot shown in Figure 3 appears to be linear with $\Delta H^{\ddagger} = 27 \pm 5$ kcal mol^{-1}, $\Delta S^{\ddagger} = 46 \pm 3$ cal mol^{-1} deg^{-1}, and $\Delta G^{\ddagger} = 13 \pm 2$ kcal mol^{-1} and also appears to be independent of substrate concentration and type.

The next two phases occur much more slowly, and thus excellent fits could be obtained over a large temperature and concentration range. Our past studies have suggested that k_{QF} (= k_{PD}) is not changed by the addition of substrates at 4 °C (*27*). Using this criterion, analysis of the data at several substrate concentrations (see below) allows assignment of one of the two slower reciprocal relaxation times from the fits to the data to the rate constant for **Q** formation (or **P** decay**)**. *Note that while this is always the second step in the reaction sequence as it was analyzed, its rate does not necessarily correlate with the second fastest reciprocal relaxation time or the phase with a positive amplitude* (evaluate eq 5 for different relative magnitude of k_{QF} and k_{QD}). The k_{QF} value measured at 4 °C is similar to that which we previously reported based on the observation of **P** decay monitored at 700 nm where it is the major contributor to the chromophore (*26*) (also see Figure 2C). As shown by the superimposed Arrhenius plots in Figure 4, both the absolute values and the temperature dependencies of k_{QF} are unchanged from the substrate-free case when methane, ethane, propane, or propene are present as substrates. This is also true for the alternate substrates furan, nitrobenzene, ethylene, and the deuterated derivatives of the alkanes previously listed (data not shown). As expected from our previous studies, values of k_{QF} throughout the temperature

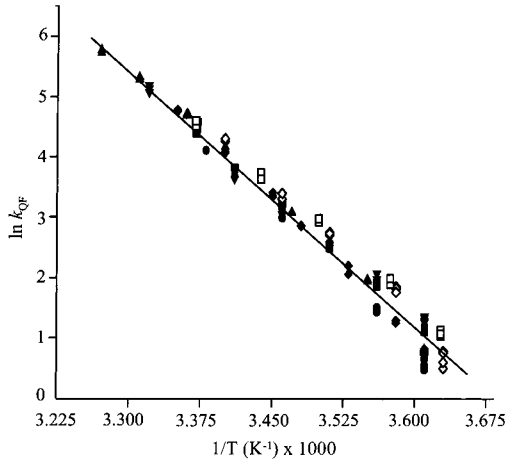

FIGURE 4: Arrhenius plot of the rate constant of **Q** formation (k_{QF}). The conditions and fitting procedure was the same as described for Figure 3 and given in Experimental Procedures. The reaction was observed for the following substrates: (♦) 100 μM methane, (■) 200 μM methane, (●) 400 μM methane, (◇) 360 μM propene, (□) 400 μM furan, (▼) 200 μM ethane, and (▲) 200 μM propane. At minimum, each experiment was performed and plotted in triplicate. The slope of the linear fit to the data was used to calculate the activation energy and other activation parameters.

range examined are unaffected by the concentration of substrate present as illustrated for the case of methane in Figure 4. The activation parameters derived from the combined Arrhenius plot are listed in Table 1. These results and those for **P*** formation reported above strongly support the proposal that most types of substrates for MMO do not interact with **P*** or **P** in a way that affects their interconversion rate constants during the process of formation of **Q**.

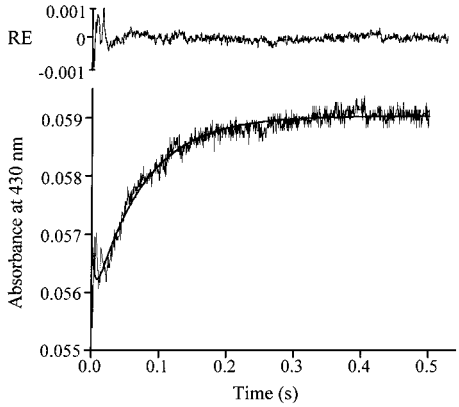

FIGURE 5: Formation of **P** in the presence of 10 mM furan. **P** formation was measured at 430 nm, pH 7, 4 °C using a single wavelength detector. The data are overlayed by a summed two-exponential fit (smooth solid line). The data shown is one of four identical experiments that were superimposable within error. Fit parameters: 430 nm: $k_1 = 40\ s^{-1}$, $Amp_1 = -0.005$; $k_2 = 13\ s^{-1}$, $Amp_2 = 0.01$. The same rate constants within error were determined for an experiment in which 15 mM furan was present and all other conditions were unchanged.

*Direct Detection of the **P** Formation Step*. One approach to the measurement of the rate constant for **P** formation is to add a large concentration of a substrate with a high rate constant for reaction with **Q** monitored at 430 nm. This effectively drives the concentration of **Q** to zero during the reaction and unmasks the weak chromophore of **P** so that the phase in which it is formed can be detected. Figure 5 shows the time course of the reaction conducted at 4 °C in the presence of 10 mM furan which reacts with **Q** with a rate constant comparable to that of methane (furan is used

Table 1: Activation Parameters for the **Q** Formation and Decay Reactions with and without Substrate

	Q formation				**Q** decay			
substrate (μM)	E_a (kcal/mol)	$\Delta H^{\ddagger}$ [a] (kcal/mol)	$\Delta S^{\ddagger}$ [a,b] (cal/mol K)	$\Delta G^{\ddagger}$ (kcal/mol)	E_a (kcal/mol)	$\Delta H^{\ddagger}$ [a] (kcal/mol)	$\Delta S^{\ddagger}$ [a,b,c] (cal/mol K)	$\Delta G^{\ddagger}$ [c] (kcal/mol)
methane								
50	29.7	29.1	50.7	14	8.9	7.6	−8.9	10.3
100-LTR	30.5	29.9	53.6	13.9	9.8	9.2	−3.4	10.5
-HTR					6.2	5.6	−20.2	10.7
150-LTR	27.7	27.1	44.1	14	12.8	12.2	6.9	10.1
-HTR					4.4	3.8	−22.4	10.5
200-LTR	25.7	26.1	37.2	15	12.9	12.3	4.4	10.3
-HTR					4.5	3.9	−21.8	10.4
400-LTR	29.3	28.7	50.3	13.7	11.9	12.5	6.8	10.5
-HTR					4.2	4.1	−21.6	10.5
d_4-methane								
200	28	27.4	44.3	14.2	11.5	10.9	−5.3	12.5
ethane								
200	27.5	26.9	43.7	13.9	15.3	14.7	16	9.9
d_6-ethane								
200	25.6	25	37.2	13.9	16.9	16.1	20.4	10
propane								
200	29.3	28.7	49.3	14	20.5	19.9	29.9	11
propene								
360	26	25.4	38.6	13.9	17.7	17.1	23.2	10.2
furan								
400	26.6	26	40.6	13.9	16.4	15.8	18.4	10.3
none	27.9	27.3	44.3	14.1	11.9	11.3	−22.6	18

[a] The error limits for the activation energy and preexponential factors that were used to determine the activation enthalpy and entropy, were ~±5% and ~±10%, respectively. [b] A temperature of 298 K was used in the ln Eying preexponential term (k_BT/h) when it was subtracted from the ln k axis intercept of the Arrhenius plots to determine the $\Delta S^{\ddagger}$ values. [c] The k_{QD} rate constants for reactions in the presence of substrates used in the Arrhenius plots are pseudo first order in substrate in most cases. Consequently, the Eyring preexponential term (k_BT/h) was multiplied by the substrate concentration before it was subtracted from the ln k axis intercept of the Arrhenius plots to determine the $\Delta S^{\ddagger}$ values. When the $\Delta S^{\ddagger}$ values determined in this way are used to calculate $\Delta G^{\ddagger}$, the values pertains to reactions with substrates at standard 1 M concentrations.

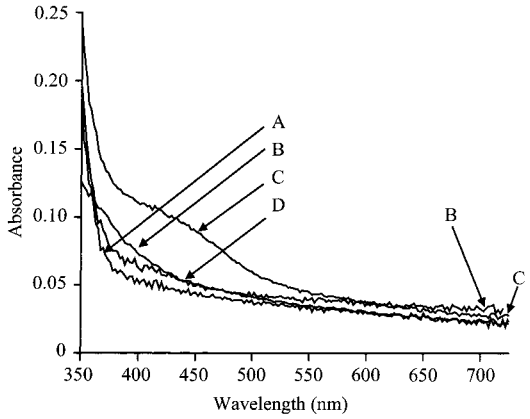

FIGURE 6: Optical spectra of transient intermediates in the reaction of $\mathbf{H^r}$ with O_2 in the absence of substrate determined by singular value decomposition fits to diode array detector data recorded at 4 °C, pH 7. A 3 component fit was used A → B → C → D. The fit yielded rate constants of 8.0, 2.5, and 0.14 s^{-1}, respectively. On the basis of these constants and the kinetic analysis from single wavelength data presented in this work, the species are assigned as **O** (and $\mathbf{H^r}$) = A, **P** = B, **Q** = C, and diferric MMOH = D.

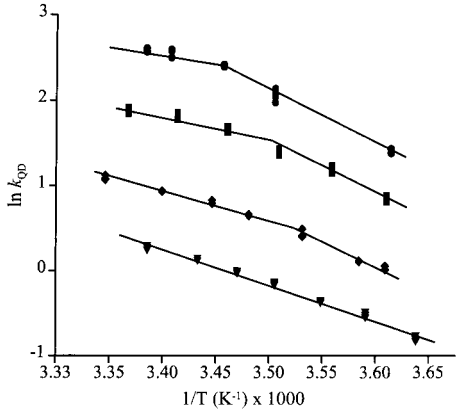

FIGURE 7: Arrhenius plot of the rate constant of **Q** decay (k_{QD}). The conditions and fitting procedures were the same as described for Figure 3 and in Experimental Procedures. Shown are the first-order rate constants from the reaction of **Q** with the following methane concentrations: (▼) 50 μM, (♦) 100 μM, (■) 200 μM, and (●) 400 μM. The fit shown (solid line) to the low and high-temperature regions for 200 and 400 μM were determined by linear regression for the points in a given range. Nonlinear Arrhenius plots were also observed for the reaction of **Q** and 150 and 300 μM methane, but were omitted for clarity.

due to its much higher solubility). Under these conditions, **Q** decays with a rate constant approximately 50 times greater than k_{QF}, so no **Q** accumulates. The time course is fit by two summed exponentials where the reciprocal relaxation time of the first negative amplitude exponential is equivalent to that measured at lower substrate concentrations. The slower positive exponential gives a rate constant of 13 ± 2 s^{-1} which is not the same as any value found in time course at low substrate concentration. However, it is comparable to the formation rate constant for **P** in the presence or absence of substrates when the reaction is monitored at 700 nm (*26*). This, considered together with the facts that **P** decay (**Q** formation), is not accelerated by furan (Figure 4) and that the amplitude of this phase accounts for the entire absorbance change between **P*** and the diferric MMOH resting state, shows that the formation of **P** is being monitored and the extinction coefficient of **P** is about the same as that of diferric MMOH at 430 nm. The low amplitude of this phase (~10% of that of **Q**) is probably why it is not observed in reactions where **Q** is formed in high yield. Accordingly, if the reaction in the absence of substrate is monitored at 540 or 700 nm where the absorbance of **Q** is greatly decreased, three phases are required to fit the time course at short times before the slow exponential phase with a reciprocal relaxation time of the **Q** decay reaction contributes significantly to the absorbance change. As shown in Figure 2C, reciprocal relaxation times of ~28, 9−12, and 2.5 s^{-1} fit the data well, suggesting that phases with reciprocal relaxation times correlating with the rate constants for **O** to **P***, **P*** to **P**, and **P** to **Q** steps are all observed.

Optical Spectra of Reaction Intermediates. Figure 6 shows the predicted optical spectra of the intermediates detected in a reaction of diferrous MMOH with O_2 in the absence of substrates. These spectra were determined through principal component analysis by singular value decomposition procedures using time-dependent optical spectra between 350 and 750 nm recorded using a diode array detector. The diode array does not have either the optical or time resolution of the single wavelength detector, so the initial fast phase was not resolved. Nevertheless, the singular value decomposition fits required a three-phase exponential equation to give an adequate simulation of the data. In this case, an additional phase is required because the absorbance changes due to the formation and decay of **P** is observable in the 700 nm region. As expected, from the analysis of the data shown in Figure 5, **P** has approximately the same absorbance as intermediate **O** and diferric MMOH at 430 nm, and the only strongly absorbing species in the 400−600 nm region is **Q**. The rate constants for the interconversion of intermediates determined from the SVD analysis were those expected from the analysis of the single wavelength experiments except for k_{QD} which approximately doubled. This is probably due to slow photoreduction of Q by the intense illumination required for diode array detection as also reported for the MMO Bath system (*37*).

Effect of Methane Concentration on the Temperature Dependence of Q Decay. Figure 7 shows the effects of methane concentration on the temperature dependence of the k_{QD} measured under the same conditions as the formation reactions shown in Figure 4. A methane concentration of 50 μM gives a nearly linear Arrhenius plot. However, nonlinear plots result at methane concentrations of 100, 150, 200, 300, and 400 μM. Temperature effects that deviate from classic Arrhenius behavior can result from many different phenomenon including thermal inactivation of the enzyme, temperature-dependent protein conformational changes, and a change in the rate-limiting step. Incubation of MMOH for more than 3 h at 24 °C resulted in no change in any of the rate constants (data not shown) ruling out thermal inactivation effects. If a protein conformational change, a change in the structure of **Q**, or a change in the MMOH and MMOB interaction is responsible for the break, then the temperature at which it is observed should be independent of substrate concentration, which is clearly not the case as shown in Figure 8 (open diamonds). Another possible origin of this effect is temperature-dependent changes in the buffer pH. In the present case, the decay of **Q** has been shown to be insensitive to pH (*26*), and the buffer used exhibits only a small change in pH with temperature (0.015 pH unit/°C).

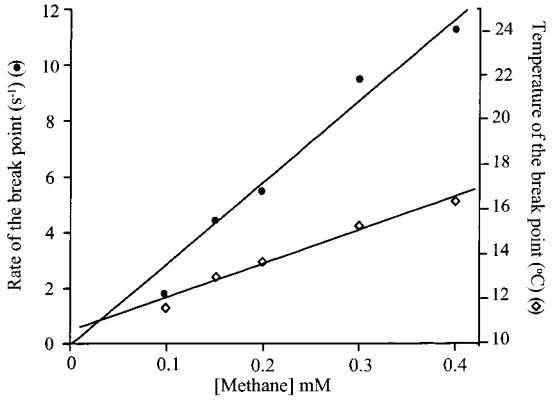

FIGURE 8: Rate and temperature of the break point from the **Q** decay Arrhenius plots as a function of methane concentration. The rate (●) and temperature (◇) at which the break in linearity occurs was determined by linear fits to data in the low and high-temperature regions of the Arrhenius plots shown in Figure 7. Data are included here for the 150 and 300 μM methane nonlinear **Q** decay Arrhenius plots which were not presented in Figure 7.

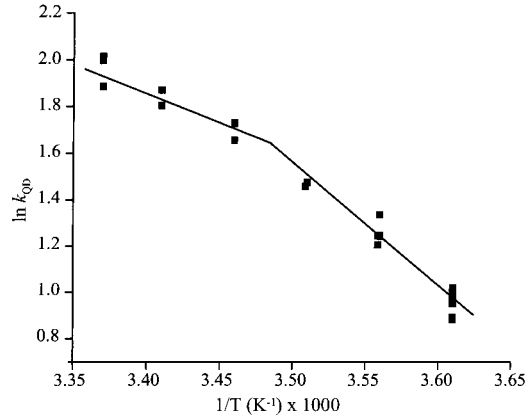

FIGURE 9: Arrhenius plot for the **Q** decay rate in a sequential mixing experiment. After an mixing $\mathbf{H^r}$ and O_2 + MMOB in the absence of methane, **Q** was allowed to build to the maximum concentration by delaying for a time interval determined by the rate constants for the reaction sequence at each temperature. Then the aged solution was mixed with 200 μM methane as in other stopped-flow experiments and the decay of **Q** was monitored at 430 nm.

Exclusion of these commonly encountered origins for nonlinear Arrhenius plots supports the possibility that there is a change in the rate-limiting step.

One possibility for a change in the rate-limiting step is that k_{QD} may become faster than one of the preceding steps in the single turnover cycle at some temperature so that the rate constant of this new slow step becomes the slowest reciprocal relaxation time of the reaction time course. In this case, it might be possible to confuse the new slow step for **Q** decay during data analysis, thereby giving rise to an apparent change in activation parameters. Indeed, this change in the rate-limiting step does occur at sufficiently high methane concentration at any given temperature. For example, for the experiments conducted using 400 μM methane at 4 °C shown in Figure 4, the **Q** decay rate constant is about 3-fold faster than its formation rate constant. Thus, the reciprocal relaxation time of the slowest exponential phase gives the **Q** formation rate constant even though this phase has a negative amplitude. This type of analysis error was not made in the current case because it would result in a uniform value for the rate constant at which the break occurs no matter what concentration of methane is present. This is true because the decay of **Q** is the only substrate concentration-dependent step (Figures 3 and 4). As shown in Figure 8 (closed circles), the rate constant at which the break occurs is not a constant but actually increases approximately linearly as the methane concentration increases. Thus, the data rule out this possible origin of the break and suggest that the nonlinear Arrhenius plot derives from multiple steps within **Q** decay reaction itself.

Plots of observed rate versus methane concentration at temperatures either below or above the break point for the data shown in Figure 7 appear linear (plots not shown). This is in accord with previous studies reported for **Q** decay data collected at 4 °C (*27*).

Decay Reaction of **Q** *in Sequential Mixing Experiments*. One method to uncouple the formation and decay reactions of **Q** during reactions with substrates so that only the latter contributes to the observed time course is to form **Q** before substrate is added using a sequential mixing strategy. In this experiment, **Q** is formed in the absence of substrate and then rapidly mixed with substrate from another set of syringes in the stopped flow device. In the absence of substrate at 4 °C, **Q** is formed about 50-fold faster than it decays, so it accumulates to nearly stoichiometric levels (*27*). As expected under these conditions, **Q** decay could be accurately fit to a single rather than triple exponential time course with rate constants similar to those determined from one phase of the single mix experiments. For example, for a reaction in which 200 μM methane was present at 4 °C, a rate constant of 2.8 s^{-1} was determined in sequential mix experiment which is in excellent agreement with the value of 2.5 s^{-1} determined from one phase of the single mix data recorded under the same conditions (data not shown). The temperature dependence of k_{QD} from sequential mix experiments shown in Figure 9 exhibits a break equivalent to that seen for the single mix experiment shown in Figure 7. This unequivocally shows that the decay rate constants and the break observed for the single-mixing stopped-flow experiments can be attributed to **Q** decay. Therefore, there must be at least two steps with different activation energy parameters in the decay process of **Q** in the presence of substrates.

Effect of Adventitious Substrates on the Temperature Dependence of **Q** *Decay*. The effects ethane, propane, propene, and furan have on the temperature dependence of k_{QD} are compared in the Arrhenius plots shown in Figure 10. As opposed to methane, the temperature dependencies of k_{QD} for these reactions give apparently linear Arrhenius plots in the accessible temperature range. The rate constants for the reactions of ethane, furan, and propene are comparable to that for methane at 200 μM where a break in the Arrhenius plot is observed. Higher concentrations of these substrates also give linear Arrhenius plots. The activation parameters for the adventitious substrates are also summarized in Table 1.

The temperature dependence of **Q** decay in the presence of deuterated methane was also examined. Deuteration should specifically affect the rate of the C−H bond breaking step, thus comparing its E_a to that of methane might reveal the region of the Arrhenius plot giving information about this chemistry. As shown in Figure 10B, the Arrhenius plot for the CD_4 reaction with **Q** is linear with an activation energy that is between those for the CH_4 reaction in the low- and

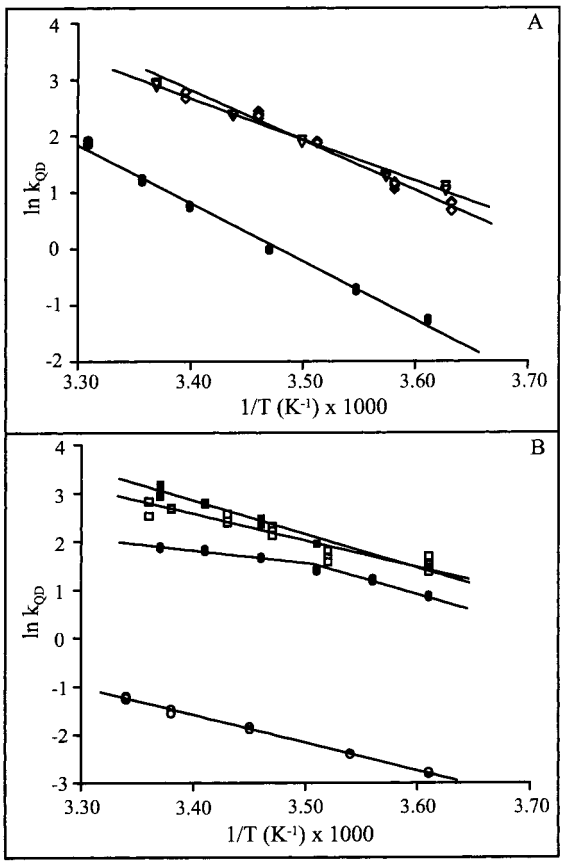

FIGURE 10: Arrhenius plots for the **Q** decay rate constant in the presence of alternate substrates. (A) Arrhenius plot of the first-order rate constants (k_{QD}) for the reactions of **Q** with (●) 200 μM propane, (◇) 360 μM propene, and (▽) 400 μM furan. (B) Arrhenius plots of k_{QD} for (■) 200 μM ethane, (□) 200 μM d_6-ethane, (●) 200 μM methane, and (○) 200 μM d_4-methane. In each panel, the solid lines are linear fits to the data sets. Each experiment was repeated in at least triplicate at every temperature.

high-temperature regions (Table 1).[3] The effect of deuteration of ethane (Figure 10B, Table 1) and propane (data not shown) were also examined. In sharp contrast, to the methane reaction with **Q**, deuteration of ethane or propane had little influence on the rate or activation thermodynamic parameters of the reaction.

DISCUSSION

Our past studies of the reaction of **Q** with substrates have focused on a single temperature or a narrow temperature range. The kinetics of the formation and decay under these conditions are fit well by considering the decay of **Q** to be a single step reaction which is first order in both **Q** and substrate. In the current study, we have shown that determination of the rate constant for **Q** decay over a wider temperature range provides evidence that at least two steps comprise the **Q** decay process as **Q** reacts with methane, suggesting an unexpected degree of complexity for the reaction. The significance of these findings is discussed in the context of previous studies of the enzyme kinetics and mechanism in the following sections.

Comparison of MMO OB3b and MMO Bath Reactions. Recently, a study of the series of reactions leading to compound **Q** formation and its subsequent reaction with substrates in the MMO Bath system was conducted using similar kinetic and thermodynamic approaches to those described here (*37*). The study confirmed many important aspects of these reactions that we have reported in studies of MMO OB3b, including: (i) the fact that the rate-limiting step switches from **Q** decay to **Q** formation as either the concentration of substrate increases (*27*) or the temperature (*35*) decreases; (ii) the lack of O_2 concentration dependence on the formation rates of the observable intermediates indicating effectively irreversible initial O_2 binding (*23*, *27*); (iii) the occurrence of at least one intermediate between $\mathbf{H^r}$ and **P** (*23*, *26*); (iv) the lack of reactivity of **P** with saturated substrates (*23*, *27*); (v) the ability of **Q** to react with all MMO substrates and an unexpected linear substrate concentration dependence of the rate constant for this reaction (*23*, *27*, *35*); and (vi) the exceptionally large deuterium kinetic isotope effect for methane reaction with **Q** (*35*). Each of these properties is in some way unusual for an enzyme reaction, but they now appear to be universal characteristics of MMO catalysis.

The recent MMO Bath experiments also revealed nonlinear Arrhenius plots[4] similar in appearance to those that we report here (*37*). However, in that case, the break was ascribed to a change in the rate-limiting step such that in the low-temperature region (LTR, $T < 17$ °C), at > 150 μM methane, **Q** formation was rate limiting, while in the high-temperature region (HTR, $T > 17$ °C) **Q** decay became rate limiting. The 420 nm data used in the MMO Bath study was fit to two or three exponential phases (depending on the temperature) but only the slowest, negative going phase was used to yield the rate data for the Arrhenius plots that exhibited the break. In the HTR, this decrease in absorbance at 420 nm was proposed to be due to **Q** decay. In contrast, in the LTR it was reported that **Q** decayed too rapidly to build up to a significant level, and this proposal was supported by the loss of methane concentration dependence on the rate constant for the negative-going phase. Instead of **Q** absorbance, the chromophore being monitored was proposed to originate from a substantial, previously undetected, absorbance of **P** (termed H_{peroxo}) which maximized near 420 nm like **Q**. In contrast to these observations, the data reported here shows that **P** lacks a substantial chromophore in this region (Figures 5 and 6). Thus, it seems unlikely to us that intermediate **P** was the species actually being followed in the MMO Bath study unless the intermediates from the different MMOH enzymes have markedly different optical properties. This conclusion is supported by several experimental observations including: (i) The rate constant for **P** formation ($9-12\ s^{-1}$ at 4 °C) has been directly measured in the absence of substrate by monitoring the absorbance from **P** at 700 nm where **P** is the major absorbing species (Figure 2C) (*26*). This same rate is observed here in the presence of a high concentration of furan because the masking absorbance of the **Q** species was eliminated by the rapid reaction of **Q** with this substrate. The low extinction coefficient of the chromophore of **P** at 430 nm revealed in this experiment was about the same as that of diferric MMOH. This is

[3] Similar conclusions were drawn in studies using MMO Bath (*37*).

[4] The temperature effects studied in the MMO Bath system were analyzed using Eyring plots. The Eyring plot is different from the Arrhenius plot only in that ln(k/T) is plotted instead of ln k, where T is the absolute temperature.

Table 2: Comparison of Activation Parameters for MMO OB3b and MMO Bath

	MMO OB3b		MMO Bath[a]	
substrate	$\Delta H^{\ddagger}$ [b] (kcal mol^{-1})	$\Delta S^{\ddagger}$ [b] (cal/mol K)	$\Delta H^{\ddagger}$ (kcal mol^{-1})	$\Delta S^{\ddagger}$ (cal/mol K)
none				
k_{QF} (k_{PD})	27.3	44.3	29.1	45
k_{QD}	11.3	−22.6	14.2	−15
150 μM CH_4				
k_{QF} (k_{PD})	27.1	44.1	28	40
k_{QD}			7.3[c]	−29[c]
k_{QD}-LTR	12.2	6.9		
k_{QD}-HTR	3.8	−22.4		

[a] Values were taken from ref *37*. [b] The error limits for the activation energy and preexponential factors that were used to determine the activation enthalpy and entropy, were ∼±5% and ∼±10%, respectively. [c] Linear Eying plots were found in sequential-mixing stopped-flow experiments similar to those presented in Figure 9 in this study.

reasonable because both species are proposed to have diferric clusters. (ii) In accord with the conclusion that **P** has little absorbance at 430 nm, we found no phase in the reaction time course with a reciprocal relaxation time that matched the known rate of **P** formation, suggesting that it is essentially isosbestic with the preceding and final species of the reaction. A change in extinction coefficient of the magnitude reported for **P** in MMO Bath would have given rise to an easily detected effect on the reaction time course. (iii) Diode array data deconvoluted into spectra of the intermediates confirm that **P** absorbs only weakly in the 420−430 nm region. This differs from the comparable SVD analysis of diode array spectra reported for **P** from MMO Bath, but the latter preparation contained a heme contaminant that partially masks the 420−430 nm region complicating the assignment of the **P** spectrum.

If **P** was not the species being followed in the MMO Bath experiments, what was? It seems likely from the current results that the absorbance at 420−430 nm is always due to **Q**. Although the observed maximum absorbance from **Q** drops steadily as the concentration of substrate increases, it is easily observable in the presence of 500 μM methane. The fact that the rate of **Q** decay may easily exceed the rate of **Q** formation in the LTR means that the rate constant for the formation reaction may be given by the reciprocal relaxation time of the negative-going (slowest) exponential. Consequently, if one uses only the negative-going exponential data, it will reflect the rate of **Q** formation (and **P** decay) in this case and would not be expected to exhibit a concentration dependence on methane as observed in the MMO Bath experiment. Conversely, the rate constant that derives from the positive going exponential under these conditions describes the **Q** decay reaction and will show a concentration dependence, as we have demonstrated here. No matter whether one ascribes the delta absorbance component of the negative-going exponential to **P** or to **Q**, the underlying reaction is the same, and it will exhibit the same energy of activation. Accordingly, the activation energies for this step are very similar for the enzymes from the two bacterial sources as shown in Table 2.

Another difference between the MMO Bath and MMO OB3b results is that the rates of **P** and **Q** formation are reported to be much slower for MMO Bath (**P**, 1−2 s^{-1}; **Q**, 0.45 s^{-1}) than MMO OB3b (**P**, 9−12 s^{-1}; **Q**, 2.4 s^{-1}) at 4 °C, pH 7 (*26*, *37*). While the slower rate of MMO Bath **Q** formation is apparent from the longer time required for **Q** to maximize in the reaction time course, the slower rate of **P** formation is more difficult to demonstrate directly and subject to interpretation of the origin of the chromophore at 420 nm. If we are correct that **P** forms comparatively rapidly and has only a weak optical spectrum, then it would have been very difficult to determine the **P** formation rate from reaction time courses at zero or low substrate concentration monitored at 420 nm. A better approach is that which we used for the data shown in Figure 5 where a high substrate concentration is used to cause **Q** to decay very rapidly, making **P** formation rate limiting and unmasking its weak absorbance. Accordingly, a similar experiment was carried out in studies of the MMO Bath system using acetylene as a high concentration substrate and showed much faster rates for both **P** formation (∼4.5 s^{-1}) and decay (∼0.85 s^{-1}) at 4 °C [see Figures S5 and S6 in (*37*)]. If these higher rates pertain, then the sequential mix experiments designed to show that MMO Bath **P** reacts directly with substrates such as propene (*37*), may require reexamination because substantially more **Q** would be formed than anticipated during the time between mixing events designed to maximize **P**. Because **Q** absorbs so much more strongly than **P**, even a small amount of **Q** will dominate the observed kinetics. Indeed, the same rate constant (∼10 s^{-1} at 20 °C) was reported for the reactions of 1 mM propene with either MMO Bath **P** or **Q** in sequential mix experiments [see Figures 8 and 9 in (*37*)]. Thus, we speculate that **Q** rather than **P** decay was being monitored in each case. In our experiments (Figure 4), we could find no evidence for direct reaction of **P** with substrates including propene. Although such a reaction seems feasible, the rate of conversion to **Q** is apparently too fast to allow this alternative chemistry.

Origin of the Break in the Arrhenius Plot for Q Decay. It is shown here that when the phase with the reciprocal relaxation time truly associated with **Q** decay is selected, the Arrhenius plot exhibits a break at a rate determined by the methane concentration. This is the first indication that the reaction of **Q** with substrates occurs in a manner other than a single step.

Although we do not yet have sufficient information to definitively state the nature of the multiple steps in **Q** decay, the reaction can be characterized to an extent that may be useful in gaining a better understanding of this remarkable chemistry. The key observations can be summarized as follows. (i) both the LTR and the HTR of Arrhenius plot exhibit substrate concentration dependent rates, thus the rate limiting reaction must be directly or indirectly coupled to substrate addition. (ii) At least one region of the Arrhenius plot (and possibly both) exhibit a large isotope effect for methane. Consequently, the rate-limiting step in this region(s) is likely to be C−H bond breaking rather than methane binding. (iii) The Arrhenius plot for CD_4 is linear and gives activation parameters between those of the HTR and LTR of the CH_4 reaction. (iv) Neither a break in the Arrhenius plot nor an isotope effect is observed for the ethane (or any substrate other than methane) reaction with **Q**, suggesting that a step other than C−H bond breaking is rate limiting. (v) The substrate concentration dependence at any given temperature is apparently linear rather than hyperbolic for all substrates. (vi) As the methane concentration is decreased,

the break point shifts to lower temperature and eventually, the Arrhenius plot becomes nearly linear with an activation energy that is approximately the average of those for the LTR and HTR of reactions that exhibit a break.

The simplest type of reaction scenario that could account for the **Q** reaction with methane and other substrates under all conditions is illustrated in Scheme 3A, where it is proposed that two steps and two substrate molecules are involved in the **Q** reaction. These steps must have different activation parameters so that the rate-limiting step changes with temperature. Throughout the temperature range, however, the chromophoric change occurs during the second step as the **Q**-substrate complex converts to the product complex. There are many possible ways in which this scheme could be implemented by the enzyme. For example, the dimeric enzyme has two active sites, so it is possible that both sites must be occupied before a reaction can occur. Alternatively, there may be an effector site that opens a channel to the diiron cluster in the normally completely inaccessible active site region. It is also possible that two substrates must bind in one active site for some reason before the reaction can occur.[5,6]

Scheme 3: Hypotheses for the Reaction of **Q** with Substrates

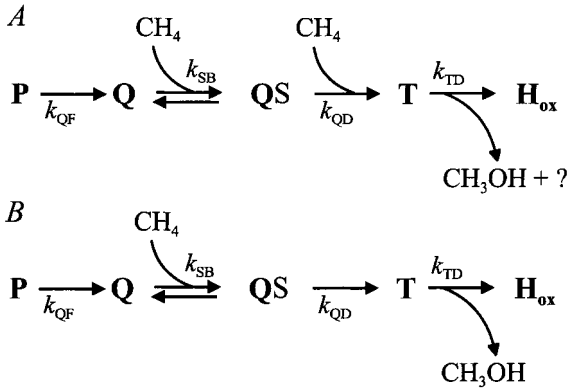

Kinetically, the binding of the second substrate in Scheme 3A converts what would normally be a hyperbolic dependence on substrate concentration into the linear response that is actually observed. Although the binding of a second substrate molecule would ensure a linear dependence on substrate concentration, it remains a possibility that a mechanism such as that illustrated in Scheme 3B pertains in which only one substrate is involved in the reaction. This would require the substrate concentration to be low relative to the K_d for binding, thereby keeping the observed rate of **Q** decay in the linear portion of what is actually a hyperbolic substrate concentration dependence. However, we have previously shown that the K_m for substrate binding is 12 μM for methane (*35*). To the extent that K_m is reflective of the substrate dissociation constant, this value suggests that the substrate concentrations used in this study (50−400 μM) are probably not significantly less than the K_d for substrate binding, favoring the requirement for two substrates illustrated in Scheme 3A. If the first methane binding reaction step is irreversible, then a methane must add in each step in order to yield the observed concentration dependence in both the LTR and HTR. The reversible methane binding reaction in step 1 of Scheme 3 couples the two rate constants so that both will have a substrate concentration dependence if substrate adds in the first step. However, the dependence of k_{QD} will be nonlinear if no substrate binds in step 2 except under the limiting conditions discussed above.

In the case of methane, Scheme 3A predicts substrate addition in the bond breaking step, directly accounting for the observed isotope effect. It is likely that a much smaller effect would be observed if the substrate binding reaction could be compared for the CH_4 and CD_4 reactions, but we believe that it is not possible to make this comparison for reasons that will be discussed below. In the case of the CD_4 reaction with **Q**, the C−D bond breaking and oxygenation reaction is likely to be rate limiting at all temperatures, so the Arrhenius plot would be expected to be linear as observed. For substrates other than methane, the binding reactions in step 1 of Scheme 3 must be assumed to be rate limiting while the oxygenation reactions are fast in accord with the lower bond energy of these substrates. The result would be a loss of both the isotope effect and the break in the Arrhenius plot, but the rate versus substrate concentration plots would still be linear. The reason for this is that the rapid conversion of the **Q**-substrate complex to the product complex **T** causes the binding reaction to be essentially irreversible and first order in substrate.

Scheme 3A was simulated using numerical integration for different temperatures and substrate concentrations as described in Experimental Procedures. The resulting time courses were then fit under the assumption that the **Q** decay occurs in a single phase as was done for the real data. The simulation successfully reproduces the break in the Arrhenius plots at high methane concentrations, the progressive shift in the position of the break, and the nearly linear plot at low methane concentration as shown in Figure 11. A plot of the predicted rate versus substrate concentration using the data from this simulation is linear as observed for the actual experiment. It is likely that the apparent loss of the break in the Arrhenius plot at low substrate concentration is due to a breakdown in pseudo-first-order conditions. However, this condition is not required for evaluation of Scheme 3A by numerical integration techniques, leading to the excellent simulation at all methane concentrations shown in Figure 11.

Significance of the Observed Activation Parameters. All of the activation parameters shown in Table 1 for the formation of **Q** (decay of **P**) are approximately the same, $\Delta G^{\ddagger} = \sim 14$ kcal/mol, independent of the type of substrate added or even whether substrate is present at all. This is the expected result if **P** does not react with substrate as proposed here. The $\Delta H^{\ddagger}$ of ∼28 kcal/mol is reasonable for an elongation of the O−O bond in the transition state, but there is actually no precedent for the energetics of such a reaction

[5] In principle, the steady-state kinetics observed for some scenarios encompassed by Scheme 3 would yield nonlinear Lineweaver-Burk plots because two CH_4 molecules would add before an irreversible reaction occurs. Only linear plots are observed; however, the actual observation of nonlinear plots will depend on several factors, especially the relative magnitudes of the steady-state kinetic K_m and K_i values for the substrates.

[6] Some evidence in favor of the need for 2 dinuclear iron clusters for efficient catalysis can be found in the observation that MMO OB3b and MMO Bath preparations containing only 1 cluster per enzyme are as much as 20-fold less active than MMO OB3b purified with 2 clusters (*3*).

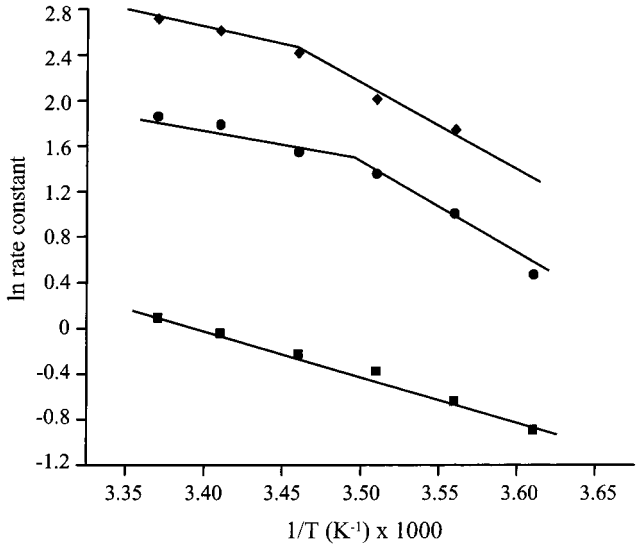

FIGURE 11: Simulations of Arrhenius plots from the kinetic model shown in Scheme 3.

occurring in a dinuclear iron cluster, so such comparisons are difficult to make except through calculations.[7] The $\Delta S^{\ddagger}$ values for this reaction are large and positive, consistent with a decrease in order as the transition state is formed. This is unexpected from the point of view of moving toward the more rigid diamond core structure of **Q**, assuming that this structure is the direct product of the reaction. However, our previous studies are consistent with release of water prior to formation of the diamond core (*26*), so the $\Delta S^{\ddagger}$ may be dominated by the increased motional disorder of the two oxygens as the transition state is approached.

In comparison to the **Q** formation reactions, all of the reactions of **Q** with substrates have low $\Delta H^{\ddagger}$ values. The comparative small values for $\Delta H^{\ddagger}$ in these steps that appear to involve breaking the C−H bond of methane is somewhat surprising. On the other hand, it may reflect the state of activation of the reactive oxygen in **Q**, the most reactive oxidizing species known in biological systems.

The $\Delta G^{\ddagger}$ values determined for methane in both the LTR and HTR as well as those of several other "fast" substrates are very similar after the rate constants that are used in the Arrhenius plot are normalized for the substrate concentration (see Table 1 footnote). Significantly greater differences, however, are found in the $\Delta H^{\ddagger}$ and $\Delta S^{\ddagger}$ for these reactions, suggesting that they have somewhat different ground states and/or transition states. The reactions with CH_4 in the HTR and LTR have rather different values for $\Delta H^{\ddagger}$ and both the magnitude and sign of $\Delta S^{\ddagger}$ are different. This result seems to be consistent with a reaction like that depicted in Scheme 3 where the two reactions involving methane are fundamentally different.

More insight into the nature of the reactions in the LTR and HTR can be gained by considering the reaction with CD_4. The $\Delta H^{\ddagger}$ and $\Delta S^{\ddagger}$ values for the **Q** reaction with this substrate are between those for the LTR and HTR for the CH_4 reaction, and the $\Delta G^{\ddagger}$ value increases substantially, consistent with the large deuterium KIE. This KIE would be expected to manifest itself primarily in an increased $\Delta H^{\ddagger}$ for the reaction,[8] suggesting that the CD_4 reaction should be compared with lower value of the CH_4 reaction represented in the HTR. Also, both the rate-limiting reaction in the HTR and the CD_4 reaction have negative $\Delta S^{\ddagger}$ values. Accordingly, if a mechanism like that depicted in Scheme 3 pertains, the activation parameters for the HTR would apply to the C−H bond breaking step and those in the LTR to the substrate binding step. The other MMO substrates, which do not exhibit a KIE for the **Q** decay reaction, all elicit positive $\Delta S^{\ddagger}$ values and the observed $\Delta H^{\ddagger}$ values are comparable to, or larger than, those observed for the LTR of the methane reaction. This is the expected result if the reaction monitored is primarily the substrate binding reaction for these alternate substrates. Moreover, the $\Delta H^{\ddagger}$ values increase slightly as the chain length of the hydrocarbon substrate increases which is not compatible with C−H bond breaking if the strength of the bond is the determining factor. Positive $\Delta S^{\ddagger}$ values for the binding of hydrophobic substrates are reasonable because organized solvent is being released during the transition state. Conversely, a negative $\Delta S^{\ddagger}$ during the putative bond breaking reaction may indicate that the two nonpolar reactant molecules become polar during the transition state requiring solvent organization. Such an increase in polarization would be expected in the transition-state hydrogen atom abstraction reaction as we have proposed for the reaction catalyzed by MMO (*4*).

Further consideration of the data in the light of the above discussion in the context of Scheme 3 addresses some unexplained observations from past studies. As illustrated in Scheme 4, Scheme 3 suggests that all substrates will yield a break in the Arrhenius plot at some temperature as long as

Scheme 4: Hypothetical Arrhenius Plots for Methane and Ethane Reactions with **Q** Based on the Reaction Sequences Shown in Scheme 3[a]

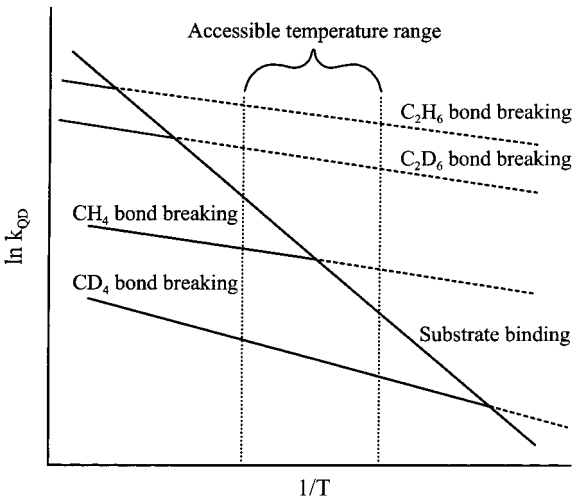

[a] For simplicity, it is assumed that the substrates have the same binding thermodynamic activation parameters.

[7] Recent density functional calculations yield similar activation parameters for both the **Q** formation reaction and the reaction of **Q** with substrates. See ref. (*40*) and Per Siegbahn, personal communication.

[8] A comparison of the $\Delta H^{\ddagger}$ values for the CH_4 and CD_4 reactions shows a larger difference than expected based on zero point energies. This may represent a complexity of this reaction that we do not currently understand. On the other hand, it may also represent a tunneling contribution as has been suggested by our previous studies (*35*) and other recent studies of oxygenase mechanisms (*41*−*43*).

the binding reaction has different activation parameters than the C−H bond breaking reaction. No break is seen in the reaction with CD_4 because the reaction cannot be monitored at a low enough temperature to allow the binding reaction to become rate limiting. The isotope effect for the reaction is best measured at temperatures above the break where the C−H bond cleaving reaction is rate limiting for both CH_4 and CD_4 reactions. Conversely, the reactions with the adventitious MMO substrates give linear Arrhenius plots because they cannot be measured at a high enough temperature to allow the C−H bond breaking reaction to become rate limiting. If this temperature could be exceeded, then an isotope effect would be observable. Whether observed in the **Q** decay kinetics or not, the reaction must nevertheless proceed through the bond breaking step in Scheme 3, leading to an overall isotope effect. This may explain why a deuterium isotope effect is observed for ethane oxidation in the product distribution (*36*) but not in the reaction of ethane with **Q** monitored at 430 nm (Figure 10B). This interpretation also accounts for the remarkable fact that the C−H bond breaking rate correlates very poorly with C−H bond energy for MMO reactions; methane is a far better substrate than propane, for example. The current hypothesis would suggest that at the temperatures the reaction can be observed, the weaker C−H bonds of longer chain hydrocarbons are, in fact, cleaved faster than that of methane. However, only in the case of methane oxidation is the actual C−H or C−D bond cleaving reaction rate limiting at accessible temperatures. For all other substrates, binding rather than C−H bond breaking is actually being observed, and thus two different types of reactions have been compared in past analyses.

REFERENCES

1. Dalton, H. (1980) *Adv. Appl. Microbiol. 26*, 71−87.
2. Anthony, C. (1982) *The Biochemistry of Methylotrophs*, Academic Press, London.
3. Fox, B. G., Froland, W. A., Dege, J. E., and Lipscomb, J. D. (1989) *J. Biol. Chem. 264*, 10023−10033.
4. Wallar, B. J., and Lipscomb, J. D. (1996) *Chem. Rev. 96*, 2625−2657.
5. Patel, R. N. (1984) in *Microbial Growth on C_1 Compounds* (Crawford, R. L., and Hanson, R. S., Eds.) pp 83−90, American Society for Microbiology, Washington, DC.
6. Nakajima, T., Uchiyama, H., Yagi, O., and Nakahara, T. (1992) *Biosci., Biotechnol., Biochem. 56*, 736−740.
7. Pilkington, S. J., and Dalton, H. (1990) *Methods Enzymol. 188*, 181−190.
8. Woodland, M. P., and Dalton, H. (1984) *J. Biol. Chem. 259*, 53−59.
9. Feig, A. L., and Lippard, S. J. (1994) *Chem. Rev. 94*, 759−805.
10. Fox, B. G., Shanklin, J., Somerville, C., and Münck, E. (1993) *Proc. Natl. Acad. Sci. U.S.A. 90*, 2486−2490.
11. Shanklin, J., Achim, C., Schmidt, H., Fox, B. G., and Münck, E. (1997) *Proc. Natl. Acad. Sci. U.S.A. 94*, 2981−2986.
12. Bollinger, J., Jr., Edmondson, D. E., Huynh, B. H., Filley, J., Norton, J. R., and Stubbe, J. (1991) *Science 253*, 292−298.
13. Nordlund, P., Sjöberg, B. M., and Eklund, H. (1990) *Nature 345*, 593−598.
14. Small, F. J., and Ensign, S. A. (1997) *J. Biol. Chem. 272*, 24913−24920.
15. Colby, J., and Dalton, H. (1978) *Biochem. J. 171*, 461−468.
16. Rosenzweig, A. C., Frederick, C. A., Lippard, S. J., and Nordlund, P. (1993) *Nature 366*, 537−543.
17. Elango, N., Radhakrishnan, R., Froland, W. A., Wallar, B. J., Earhart, C. A., Lipscomb, J. D., and Ohlendorf, D. H. (1997) *Protein Sci. 6*, 556−568.
18. Fox, B. G., Surerus, K. K., Münck, E., and Lipscomb, J. D. (1988) *J. Biol. Chem. 263*, 10553−10556.
19. Lund, J., and Dalton, H. (1985) *Eur. J. Biochem. 147*, 291−296.
20. Fox, B. G., Liu, Y., Dege, J. E., and Lipscomb, J. D. (1991) *J. Biol. Chem. 266*, 540−550.
21. Froland, W. A., Andersson, K. K., Lee, S.-K., Liu, Y., and Lipscomb, J. D. (1993) in *Microbial Growth on C_1 Compounds* (Murrell, J. C., and Kelly, D. P., Eds.) pp 81−92, Intercept Ltd., Andover, U.K.
22. Liu, K. E., Valentine, A. M., Wang, D. L., Huynh, B. H., Edmondson, D. E., Salifoglou, A., and Lippard, S. J. (1995) *J. Am. Chem. Soc. 117*, 10174−10185.
23. Liu, Y., Nesheim, J. C., Lee, S.-K., and Lipscomb, J. D. (1995) *J. Biol. Chem. 270*, 24662−24665.
24. Liu, Y., Nesheim, J. C., Paulsen, K. E., Stankovich, M. T., and Lipscomb, J. D. (1997) *Biochemistry 36*, 5223−5233.
25. Fox, B. G., Borneman, J. G., Wackett, L. P., and Lipscomb, J. D. (1990) *Biochemistry 29*, 6419−6427.
26. Lee, S.-K., and Lipscomb, J. D. (1999) *Biochemistry 38*, 4423−4432.
27. Lee, S.-K., Nesheim, J. C., and Lipscomb, J. D. (1993) *J. Biol. Chem. 268*, 21569−21577.
28. Shu, L., Nesheim, J. C., Kauffmann, K., Münck, E., Lipscomb, J. D., and Que, L., Jr. (1997) *Science 275*, 515−518.
29. Lee, S.-K., Fox, B. G., Froland, W. A., Lipscomb, J. D., and Münck, E. (1993) *J. Am. Chem. Soc. 115*, 6450−6451.
30. McMurry, T. J., and Groves, J. T. (1986) in *Cytochrome P-450 Structure, Mechanism, and Biochemistry* (Ortiz de Montellano, P. R., Ed.) pp 1−28, Plenum Press, New York.
31. Dawson, J. H. (1988) *Science 240*, 433−439.
32. Sono, M., Roach, M. P., Coulter, E. D., and Dawson, J. H. (1996) *Chem. Rev. 96*, 2841.
33. Marletta, M. A., Hurshman, A. R., and Rusche, K. M. (1998) *Curr. Opin. Chem. Biol. 2*, 656−663.
34. Sligar, S. G., and Gunsalus, I. C. (1976) *Proc. Natl. Acad. Sci. U.S.A. 73*, 1078−1082.
35. Nesheim, J. C., and Lipscomb, J. D. (1996) *Biochemistry 35*, 10240−10247.
36. Priestley, N. D., Floss, H. G., Froland, W. A., Lipscomb, J. D., Williams, P. G., and Morimoto, H. (1992) *J. Am. Chem. Soc. 114*, 7561−7562.
37. Valentine, A. M., Stahl, S. S., and Lippard, S. J. (1999) *J. Am. Chem. Soc. 121*, 3876−3887.
38. Fox, B. G., Froland, W. A., Jollie, D. R., and Lipscomb, J. D. (1990) *Methods Enzymol. 188*, 191−202.
39. Chang, S. L., Wallar, B. J., Lipscomb, J. D., and Mayo, K. H. (1999) *Biochemistry 38*, 5799−5812.
40. Basch, H., Mogi, K., Musaev, G. D., and Morokuma, K. (1999) *J. Am. Chem. Soc. 121*, 7249−7256.
41. Kohen, A., and Klinman, J. P. (1998) *Acc. Chem. Res. 31*, 397−404.
42. Glickman, M. H., Wiseman, J. S., and Klinman, J. P. (1994) *J. Am. Chem. Soc.* 793−794.
43. Hwang, C.-C., and Grissom, C. B. (1994) *J. Am. Chem. Soc. 116*, 795−796.

BI001473L